Review of a thesis

submitted by

Dr. mont. Dipl.Ing. WALTER PURRER

Montanuniversität Leoben
(Mining University of Leoben)

February 1983

A model for computing the behaviour of a deep-seated seam roadway in basically solid rock - interspersed with planes of separation - which indicates the failure mechanisms as found in-situ and in model tests.

Experts consulted, Mining University of Leoben

o. Prof. Dr. techn. Dipl.Ing. GEORG FEDER
o. Prof. Dr. Mont. Dipl. Ing. EDUARD CZUBIK

Computation model for a deep-seated roadway in horizontal bedding.

1. Introduction

The Finite-Element-Method is increasingly used for the mathematical assessment of the complex redistribution of stresses around underground excavations. However, there are also limits to this method inspite of the fact that considerable progress was made in assessing the post-failure behaviour of the rockmass: the failure structures around a roadway in bedded rock as shown in fig. 1 and 2, could not yet be reproduced by means of the FE-programmes. Hence, the computation model described hereafter is a novel approach which seems to be better suited to the problems of deep underground excavations. In this model the rock around an excavation is divided into a solid zone (elastic zone) which, according to the theory of elasticity, can be handled with the Boundary-Element Method, and a failure zone to which we apply the failure mechanics computation method (equilibrium concept of evolving sets of failure). The latter were developed on the basis of model tests andfailure mechanisms observed in-situ.
The computation results were compared with the actual phenomena encountered and the theoretical assumptions of the model could thus be verified (calibrated).

2. Model concept

Fig. 1 shows the schematic failure pattern around a rectangular roadway after Jacobi (2). We notice that the cracks in the sidewalls due to rock pressure normal to the stratification are limited to the strata which lost their horizontal stress either through the driving operation itself (stage b) or through the failure caused by folding (stage e).
Fig. 2 shows one of the many model tests run by the Coal Mining Association of Essen (2): an originally circular roadway was subjected to pressure normal to the stratification up to stage e. It is clearly evident that the wedge failures in the sidewalls end at the folding horizon of roof and floor; the original excavation geometry (circular, rectangular or horseshoe profile) is of secondary importance.

3. Solid bedrock

3.1. Computation concept

Based on the above observations the solid bedrock outside these natural boundary planes is considered an elastic isotropic halfplane. In between there is a narrow rectangular strip of jibbed-in layers (worked rock) to which the failure phenomena are restricted. First taking the area of solid bedrock we can determine the contact stresses between the two halfplanes and the jibbed-in layers by means of a statically undetermined calculation: the statically unknown quantities are groups of stress triangles allowing for a stepwise linear approximation of any given stress course. Fig. 3 shows the breakdown of normal stresses, and fig. 4 that of shear stresses. The throw in the course of stresses between section 2 and 1 is due to the possibility of elastic stress relief gliding in area 2, which may lead to the loss of cohesion possibly existing between the seam and the surrounding rock. The method described permits to determine the depths of these gliding movements by way of simple iterations(1). The above procedure reduces the problem to determining the deformations resulting from unknown stress triangles. For the elastic isotropic halfplanes these are exactly determined by the integration of Boussineque's solution (3), cf. fig. 5 and 6. The deformations of the rectangular strip may be derived in a good approximation from the stress distribution shown in fig. 7 (1)
Here are a few deliberately oversophisticated comparative calculations-the results of which are of some interest:

3.2. Calculation results

Figures 8 - 11 show the contact stresses between the worked layers and the surrounding rock for a square roadway profile under horizontal and vertical primary pressure of 10 MN/m^2. In fig. 8 and 9 the worked rock has the same elastic properties as the roof and floor, whereas, in fig. 10 and 11 the deformation module of the rectangualr strip was reduced to 15% of that of the two halfplanes. In fig. 8 and 10 the contact surface was taken to be shear-resistent (high cohesion). The examples in fig. 9 and 11 are based on a friction coefficient of 0.3 in the absence of cohesion. This value corresponds to the shear strength in a plane of separation (2) leading to the elastic stress relief gliding of an entire bedding sequence.

Fig. 8 shows the situation in homogeneous rock. As expected, normal stresses and shear stresses are highest at the excavation edge i.e. 1.7 times the primary pressure as indicated by the dotted line (cf. circular cross-section $\sigma_t \triangleq 2.0 \times p_I$). If the worked rock has a low deformation module the direct stress on the side falls below the value prior to the excavation. Concurrently the maximum normal stress migrates to the inside of the rockmass. This is due to the fact that the shear stresses in the contact surface cause the introduction of horizontal stresses into the soft layer (seam) and thus induce transverse strain further inside the rock. Hence, the static properties of the soft layer become better and vertical stresses are attracted. This effect becomes more pronounced the lower the deformation module of the soft layer and the higher the one of the surrounding rock. Solid surrounding rock is good for preventing failure phenomena, for the greatest vertical stress occurs where the rock strength is high due to the horizontal stress obtaining in the area. With regard to rockburst (much feared in coal mining) the situation is extremely unfavourable since a coalseam can absorb a high degree of deformation energy without failing. If, in addition, the adhesion between the coalseam and the surrounding rock is very high the stress will propagate as shown in fig. 10 - which is extremely dangerous. If, for example, the interlocking force is suddenly gone due to vibrations during driving operations the state shown in fig. 11 may come about (same preconditions but no cohesion and a friction coefficient of 0.3 in the contact surface): due to a decrease in shear stress the seam sections close to the excavation will lose part of their horizontal stress. Hence, elastic deformation energy will be set free, the failure strength of the rock may suddenly become inadequate, and the dynamics of rockburst will be set under way.

These conclusions derived from calculations were fully confirmed in practical coal-mining. Further comparative computations for a non-supported rectangular roadway at the colliery of Niederberg near Duisburg (Germany) show that disregarding the low deformation module of coal would lead to an overestimation of the side stresses. Fig. 12 shows one such roadway at a depth of 300 m, where the sides are intact except for some local bursts. On the basis of existing data on rock mechanics the ratio between the deformation module of the seam and the surrounding rock (massive, banded shaly clay without planes of

separation) was estimated to be my= 0.4. The calculation in fig. 13 results in a vertical stress on the side of approximately 13 MN/ m^2 , which is slightly less than the strength of coal of approx. 15 MN/m^2.

4. Failure zone of worked rockbeds

4.1. Failure mode

A series of model tests were run in order to study the failure mode in worked rockbeds. Fig. 14, shows one of these tests in which two residual pillars were subjected to pressure(normal to the stratification) and squashed. The pillar on the left had a high friction coefficient of my = 0.8 to 1.2 with the surrounding rock, the one on the right had only 0.15 to 0.25, due to the insertion of a Teflon layer. Note the difference in the behaviour of one and the same material: scaling (slabbing) at high friction on the left, and on the right, wedge failures with smooth contact surfaces as shown in fig. 1 and 2. These test results can be obtained with a very simple mathematical procedure (fig. 15). If there is no friction with the surrounding rock we get a failure angle of 45 +φ/ 2 and a plane shear surface when applying the Mohr-Coulomb Failure-Criterion. When looking for the kinematically possible plane shear surface with a friction coefficient of my to the roof, we find that the angle of theta increases with increasing my (1) which again tallies with our obeservations. However, if the friction factor exceeds a certain value (fig. 15) the wedge will become self-locking and a plane shear surface is no longer possible. There is a flowing transition between the two extreme values i.e. from the plane wedge failure surfaces to the curved scalings in the lefthand pillar (fig. 14).

Rock brittleness is another important parameter for the failure mechanisms in worked rockbeds; it is, however, difficult to quantify. In qualitative terms, model tests and in-situ observations indicate that plastic material tends to develop curved failure planes, whereas, in brittle rock the typical failure structures (Riedel-failure, shear zones instead of shear surfaces) will develop in accordance with the possible failure mechanics. This possibility of evading pressure is given in the mechanism of wedge failure described in the following:

4.2. Computation concept (mechanism of wedge failure)

Fig. 16,shows the computation concept for the wedge failure zone which consists mainly in examining the equilibrium of forces acting upon the wedges. These are dependent on the residual shear-strength of coal, the friction with the surrounding rock and on the stiffness of the surrounding rock itself since it determines the amount of induced deformation,and hence, the magnitude of force Pu,acting upon the tip of the wedge. Tests on coalwedges showed that independent of the mean horizontal stress in the seam the stress at the tip of the wedge is slightly higher than the uniaxial compressive strength (1). This measured result is not contradictory to the theory of Mohr-Coulomb, and by carefully analyzing the failure process it can be explained as follows: due to the volume expansion of broken rock there is a concentration of horizontal stress inthe immediate vicinity of the zones of clastic failure or structural failure (fig.18). The result is a local arching effect through which the major part of vertical stresses is transmitted to the adjacent wedges by friction on the wedge flanks, whereas, only the share corresponding to the cohesion of the material is directly acting upon the flattened tip of the wedge. The two shares taken together allow for a fulfillment of the Mohr-Coulomb condition at any point in time above the intersection s (fig.18) which one can imagine as the midline through the interface between crushed zone and solid rock. It follows from this that a higher horizontal stress in the seam leads to an increase of the share of friction transmitted via the wedge flanks without changing the amount of cohesion transmitted directly at the tip of the wedge.

5. Coupling of failure zone and solid rock

In the computation model the forces of the mutually pushing wedges are coupled with the surrounding solid zone in that the borderline to elastic rock is progressively deferred until the failure zone and its residual strength are high enough to prevent further wedge failure. In the example shown in fig. 19, the a.m. Niederberg roadway was theoretically changed from 300 m to 1000 m of depth. The data relating to the strength of coal used in the computation are shown in fig. 20.

With a roadway width of 5.50 m, a seam thickness of 2.50 m the resulting depth of the wedge failure zone is 3.40 m (area 3) followed by a 1m wide zone of elastic stress relief gliding (fig. 19).

6. Behaviour of roof and floor

A largely elastic behaviour of the surrounding rock (elastic isotropic halfplane) is a precondition to the example shown in fig. 19. There are, however, relatively few roadways where the failure occurs in the sidewalls alone. Moreover, the following two examples show that applying contiunuum mechanics to the surrounding rock is inadequate for assessing the stability and/or the onset of failure in roof and floor:

a) In South African gold mines there are excavations of only 1 m in height but 100 in width. With such an excavation geometry, and horizontal pressures amounting to 50% of the vertical ones, tensile cracks would inevitably be expected in the roof. And yet, reality is different: width of span up to 100m without failure are possible, roof and floor show no tensile cracks and the deformations are 2 to 4 times larger than in the model of continuum mechanics.

b) In coalmining we find time and again that planes of separation (bedding planes with low shear_strength) have a major influence on the stability of roof and floor.

Therefore, let us take a closer look at the stress situation in the surrounding rock: fig. 21 shows the roof of a rectangular roadway. The dotted lines delineate the areas where the interbed shear stress amounts to more than 30% of the normal stress. If a plane of separation (my=0.3) crosses that zone gliding movements are inevitable.

6.1. Computation of the influence of planes of separation near excavations with the aid of the Displacement-Discontinuity-Method

An explanation of this behaviouris easily found in the theoretical model of a rockarch (fig. 23), but there is yet another effect: fig. 24 shows that the redistribution of stresses resulting from the gliding movement along a bedding plane has an off-centre effect on the adjacent bed thus causing additional bending, and hence, inducing tensile stresses normal to the stratification. This will invariably lead to separations since there is practically no tensile strength left along the displacement. Fig.21 shows the zone where such separations (cleavage) occur. The same applies to the computation in fig. 22 where the gaping planes of separations are indicated in heavy black lines.

6.3. Conclusions drawn from the computations

Low shear-strength bedding planes in the immediate vicinity of an underground excavation have a major impact on the stress situation. It is neither correct nor reliable to compute stresses by means of the model of continuum mechanics and to attribute the increased folding tendency to the decrease in rockstrength due to stratification (common slogan: rock system strength is not equal to rock strength).

- The absence of tensile cracks in the roof of wide-span excavations can be explained by the displacements along beds of separations parallel to the stratification. We know that South-African quarzite holds bedding planes with shaly clay filling and very low shear strength.

- The separation of bedding planes also explains the greater deformations of roof and floor layers in reality as compared with the results obtained with the model of continuum mechanics.

7. Important factors in the computation of support dimensions

As far as support measures for influencing the above processes are concerned, we must consider that we are dealing with deep underground excavations where the support necessary for preventing displacements in the roof layers would exceed what is technically feasible by several powers of ten. The direct influence on the stress field may therefore be neglected. The possible increase

of rockstrength through support measures is, however, of much greater importance. In particular, the resistence of unworked rock to typical instability failure (slabbing or folding) can be multiplied by a good support system (5).

One word on the influence of the shape of an excavation: fig.15, shows the horseshoe profile with an arched roof and a plane floor section that is common in mining. The brackets projecting in the roof section are usually so deformed by bending stress that the load absorbed is small in comparison with the redistribution stresses. Therefore, we can do an approximating rectangluar computation and the bracket acts like an artificial support. As such it is in a position to prevent a folding event at least in part, as shown in this and other model tests.

8. Conclusions

The concepts underlying the development of the described computation model are similar to the analytic model worked out by Feder (5). The two models are characterized by the fact that they go from the global approach (rectangular strip between two half-planes) to the solution of detail problems (i.e. residual strength at the wedge tip). The inverse procedure, that is to conclude from the behaviour of small rock sections (i.e. laboratory specimen) as to the complex failure processes in the rock systems around an axcavation has so far not furnished satisfactory results for the following reason: in solid rock we have not only one but at least two principal failure mechanisms (shear failure and slabbing) which may also occur in combination (i.e. crushing of the tip of the wedge, chapter 4.1), and which may have a decisive influence on the post-failure behaviour of the rock. In general it is not possible to draw conclusions as to the failure mechanisms of an entire rock system around a roadway on the basis of laboratory specimen failure patterns - which depend on a great many factors some of which as yet unexplored. The example of quarzite in South-African gold mining is to illustrate this:

fig. 26 shows the failure pattern of a laboratory specimen in uniaxial compressive testing with a rigid test device. The smooth shear failure observed in that test is in sharp contrast to the brittle platy failure pattern (slabbing or cleavage) encountered in a roadway driven through the same type of rock. Therefore, it appears to be scrictly necessary to study real situations very carefully and to simulate them in model tests in order to be able to assess in quantitative terms the failure mechanisms to be expected in each case,and to arrive at realistic assumptions for the purpose of computation.

The computation model presented in this paper is by no means completed. The results obtained so far seem to indicate that the overall apporach is correct. The redistribution of stresses when folding occurs in roof and floor is still an open problem. There are some possible solutions to this problem which presuppose the running of model tests and in-situ observations underground of the type previously described with a view to translating theoretical assumptions into a realistic computation approach.

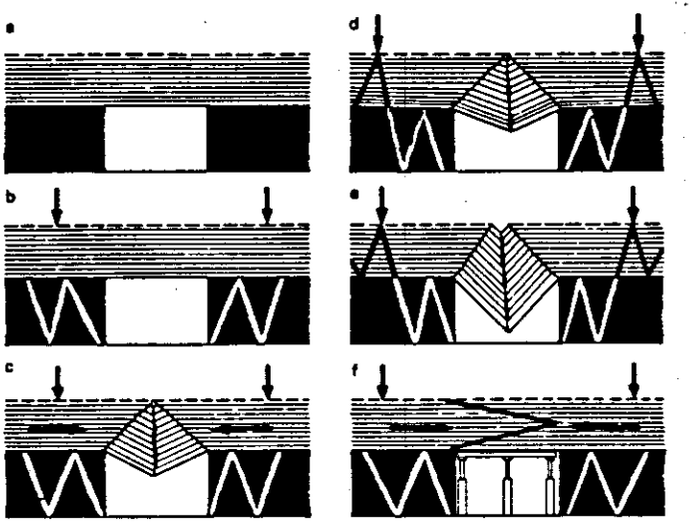

Abb. 1 Bruchablauf einer Flözstrecke in flacher Lagerung

Failure pattern of a coal seam road in horizontal bedding

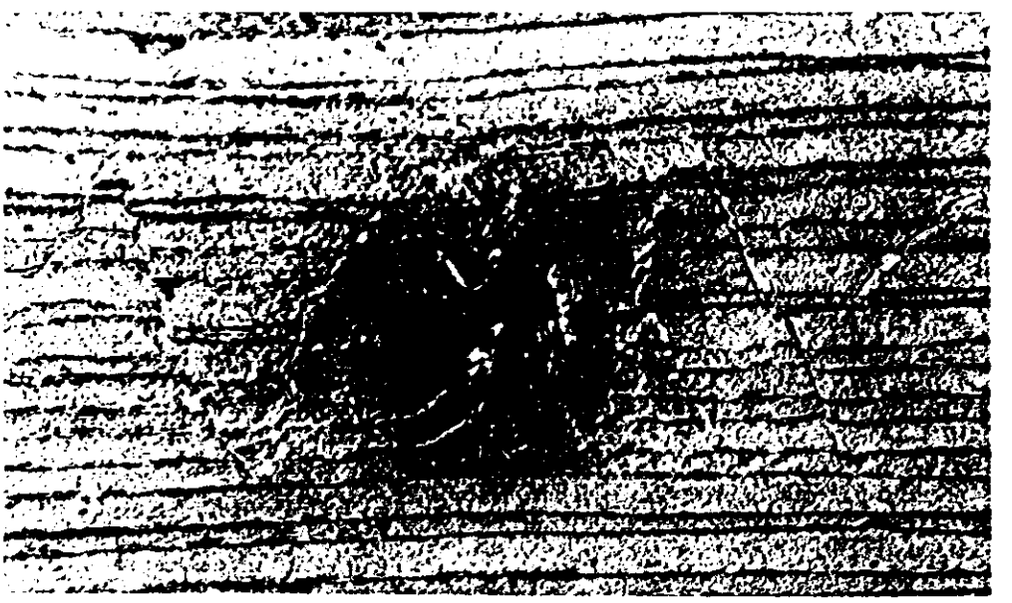

Abb. 2 Bruchbild einer Strecke im Modell nach Zischinsky (2)

Failure pattern of a model roadway after Zischinsky (2)

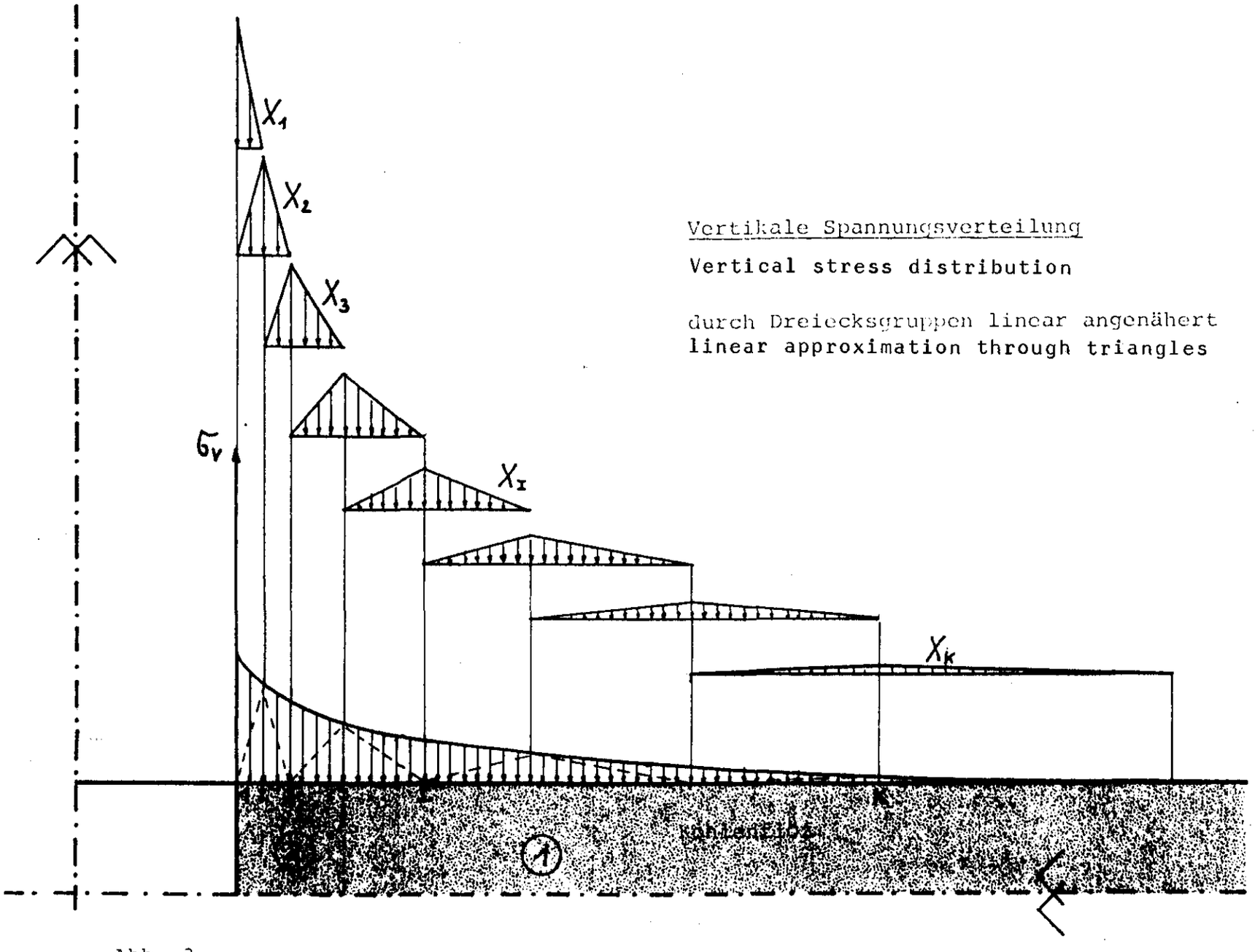

Vertikale Spannungsverteilung

Vertical stress distribution

durch Dreiecksgruppen linear angenähert
linear approximation through triangles

Abb. 3

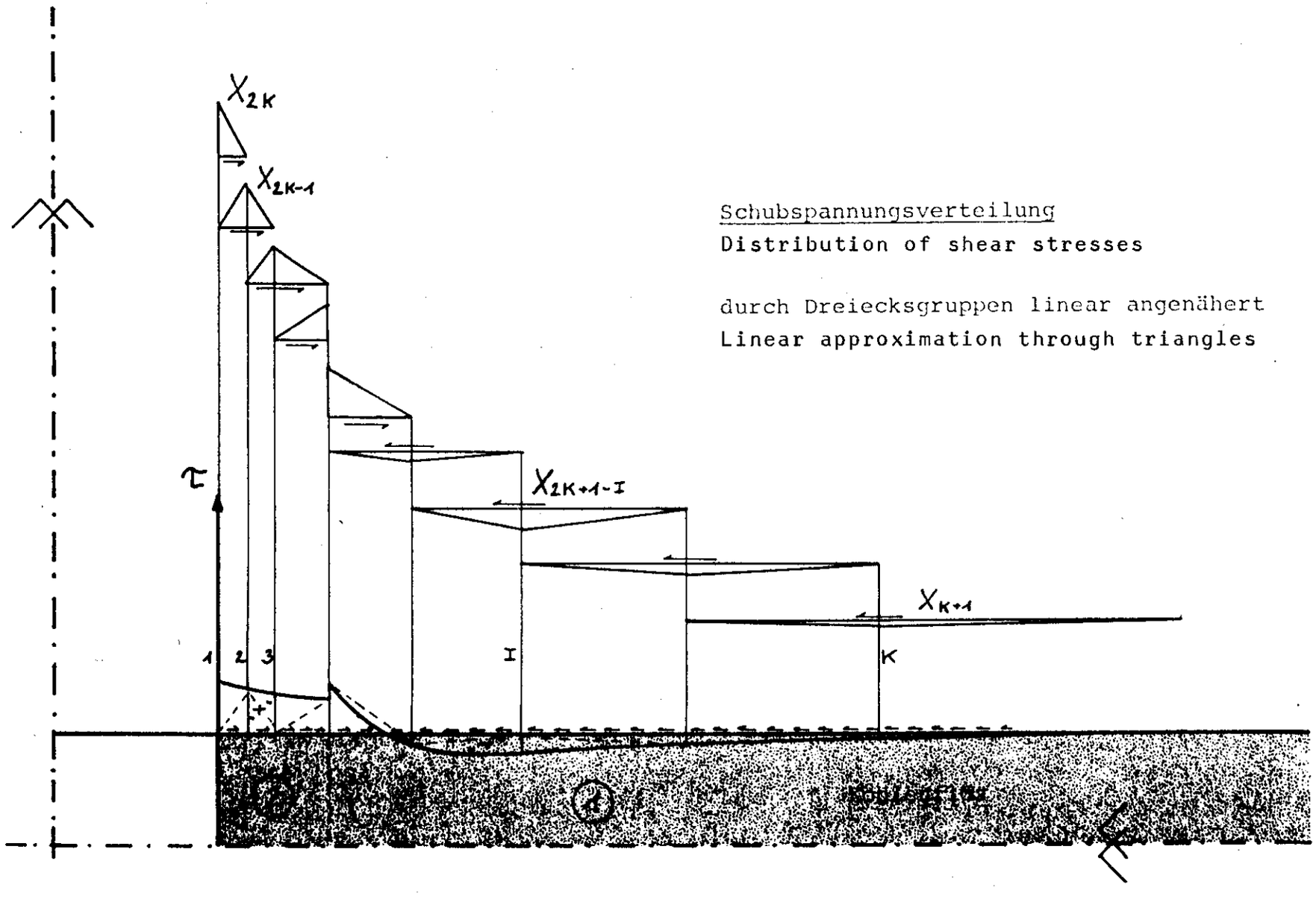

Schubspannungsverteilung
Distribution of shear stresses

durch Dreiecksgruppen linear angenähert
Linear approximation through triangles

Abb. 4

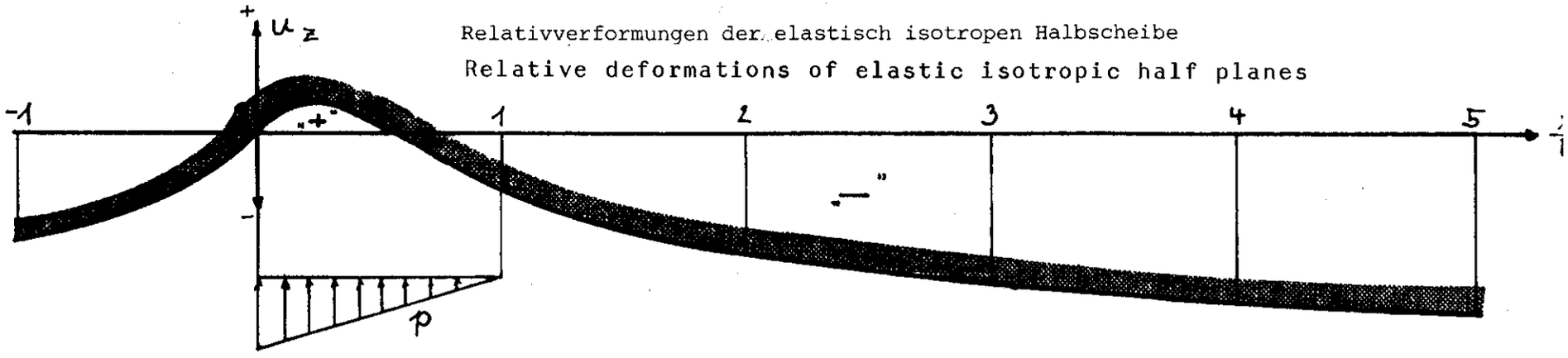

Relativverformungen der elastisch isotropen Halbscheibe

Relative deformations of elastic isotropic half planes

$$u_z = -\frac{p}{E}\,\frac{1-\nu^2}{\pi}\,b\left\{\left(1-\frac{x}{b}\right)^2 \ln\left|1-\frac{x}{b}\right| + \left[1-\left(1-\frac{x}{b}\right)^2\right]\ln\left|\frac{x}{b}\right| + \frac{x}{b}\right\} \qquad (F_3)$$

Abb. 5 Vertikalverformung infolge vertikaler Dreieckslast =
Horizontalverformung infolge Horizontallast (nicht dargestellt)

Vertical deformation due to vertical triangular load
Horizontal deformaton due to horizontal load (not shown)

Relativ deformations of the elastic isotropic half-plane

Relativverformungen der elastisch isotropen Halbscheibe

$$u_z = \frac{q}{E}(1+\nu)(1-2\nu)\,b\left[\frac{x}{b} - \left(\frac{x}{b}\right)^2 \cdot \frac{1}{2}\right] \qquad 0 < \frac{x}{b} \leq 1$$

$$u_z = \frac{q}{E}(1+\nu)\cdot(1-2\nu)\,\frac{b}{2} \qquad \frac{x}{b} \geq 1$$

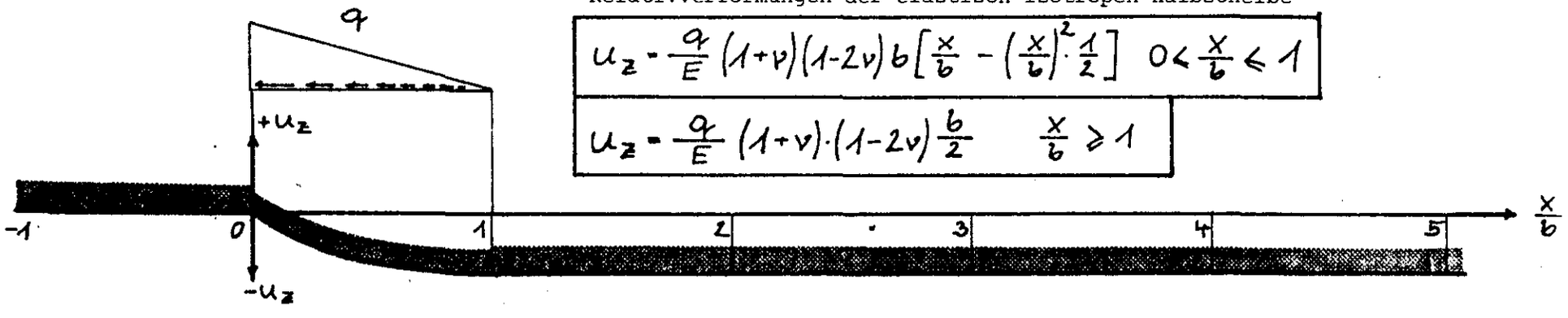

Abb. 6 : Vertikalverformung infolge horizontaler Dreieckslast = negative
Horizontalverformung infolge vertikaler Dreieckslast (nicht dargestellt)

Vertical deformation due to horizontal triangulat load = negative
Horizontal deformation due to vertical triangular load (not shown)

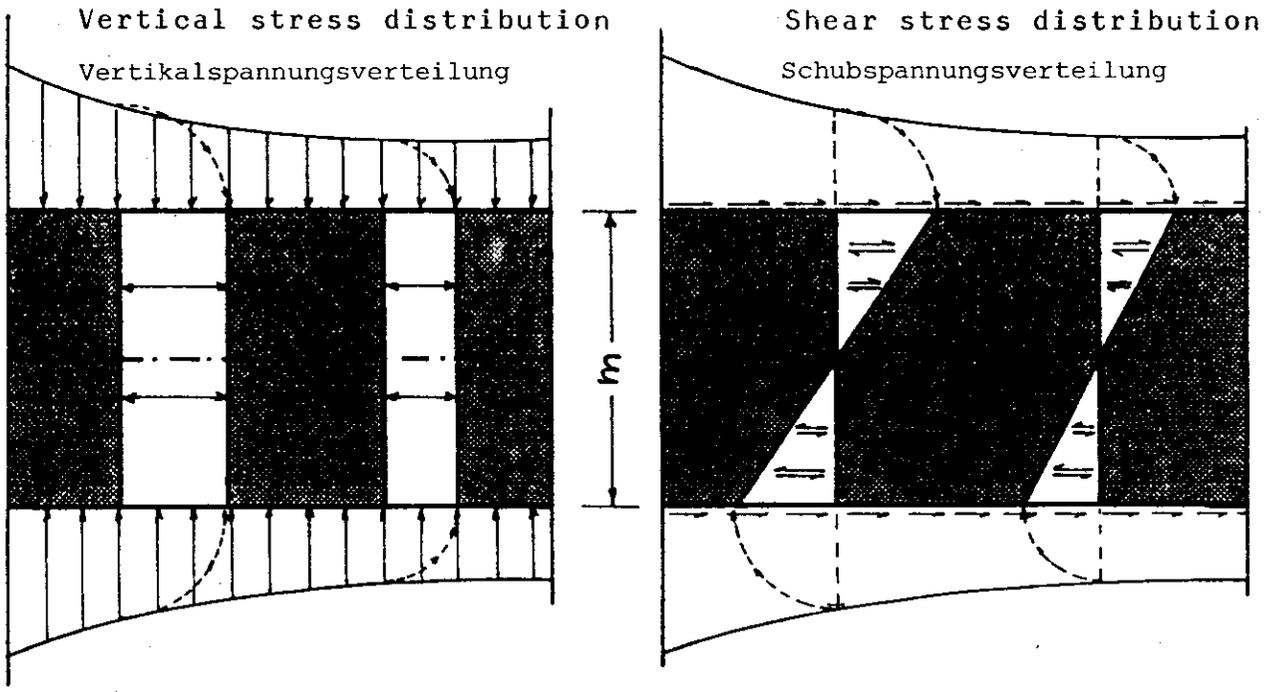

Abb. 7 Angenommene Spannungsverteilung im Rechteckstreifen (Näherungslösung)

Assumed stress distribution in rectagular strips (Approximation solution)

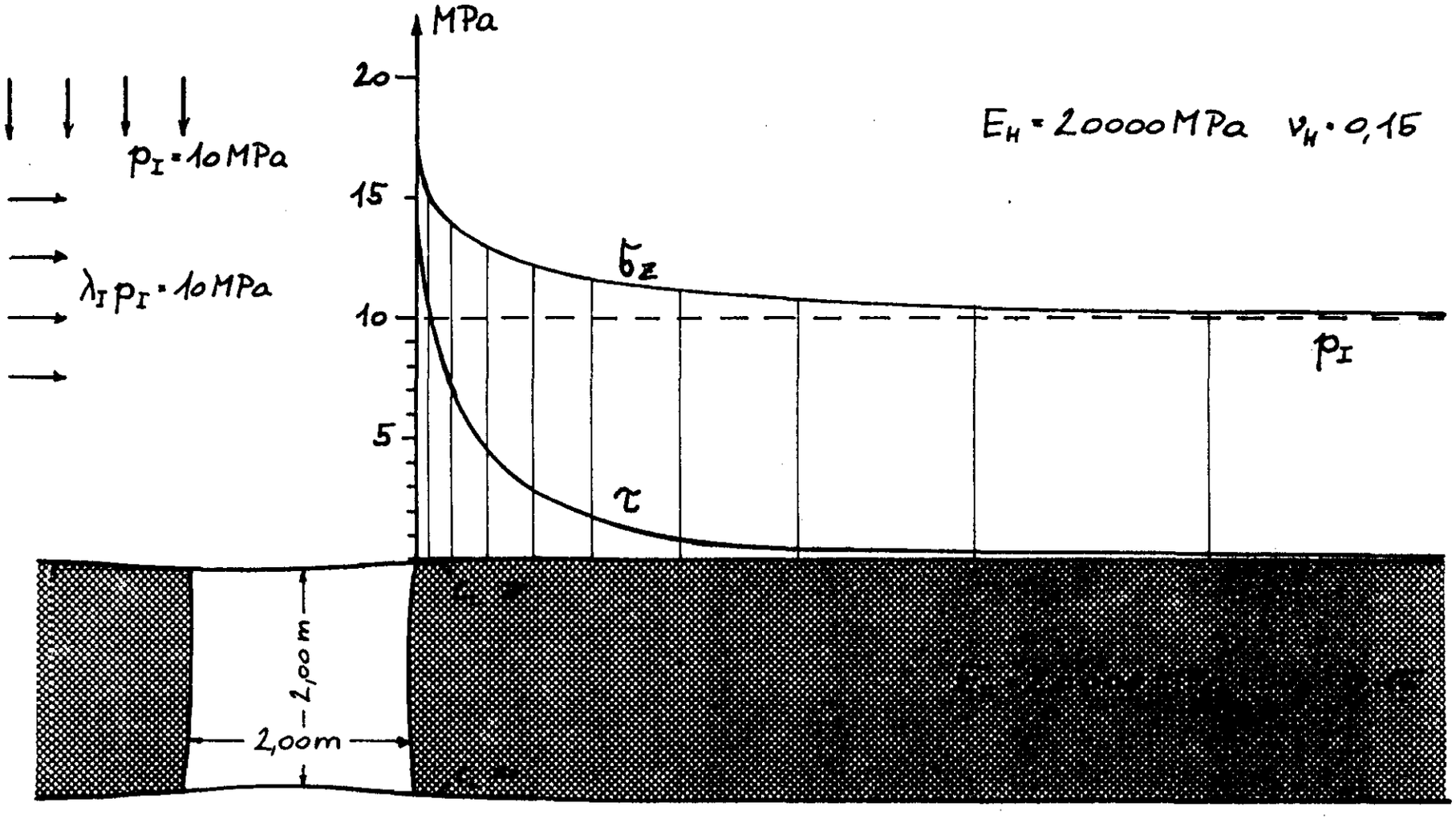
MPa
20
15
10
5
p_I = 10 MPa
$\lambda_I p_I$ = 10 MPa
σ_z
τ
p_I
2,00 m
2,00 m
E_H = 20000 MPa ν_H = 0,15
E_L = 20000 MPa ν_L = 0,15

Abb. 8

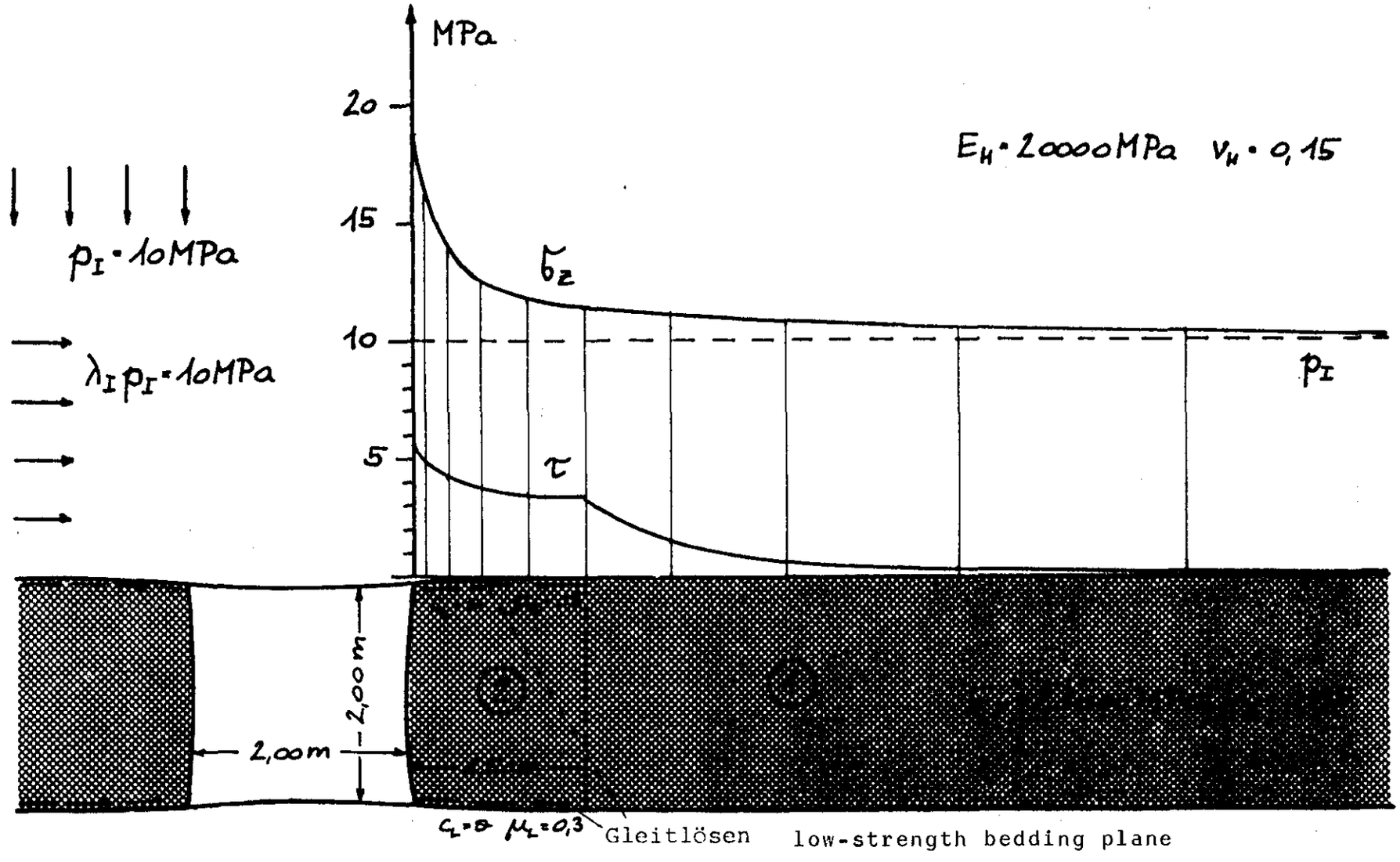
MPa
20
15
10
5
E_H = 20000MPa ν_H = 0,15
p_I = 10MPa
$\lambda_I p_I$ = 10MPa
σ_z
p_I
τ
2,00m
2,00m
c_L = 0 μ_L = 0,3
Gleitlösen
low-strength bedding plane
E_L = 20000 MPa ν_L = 0,15

Abb.9

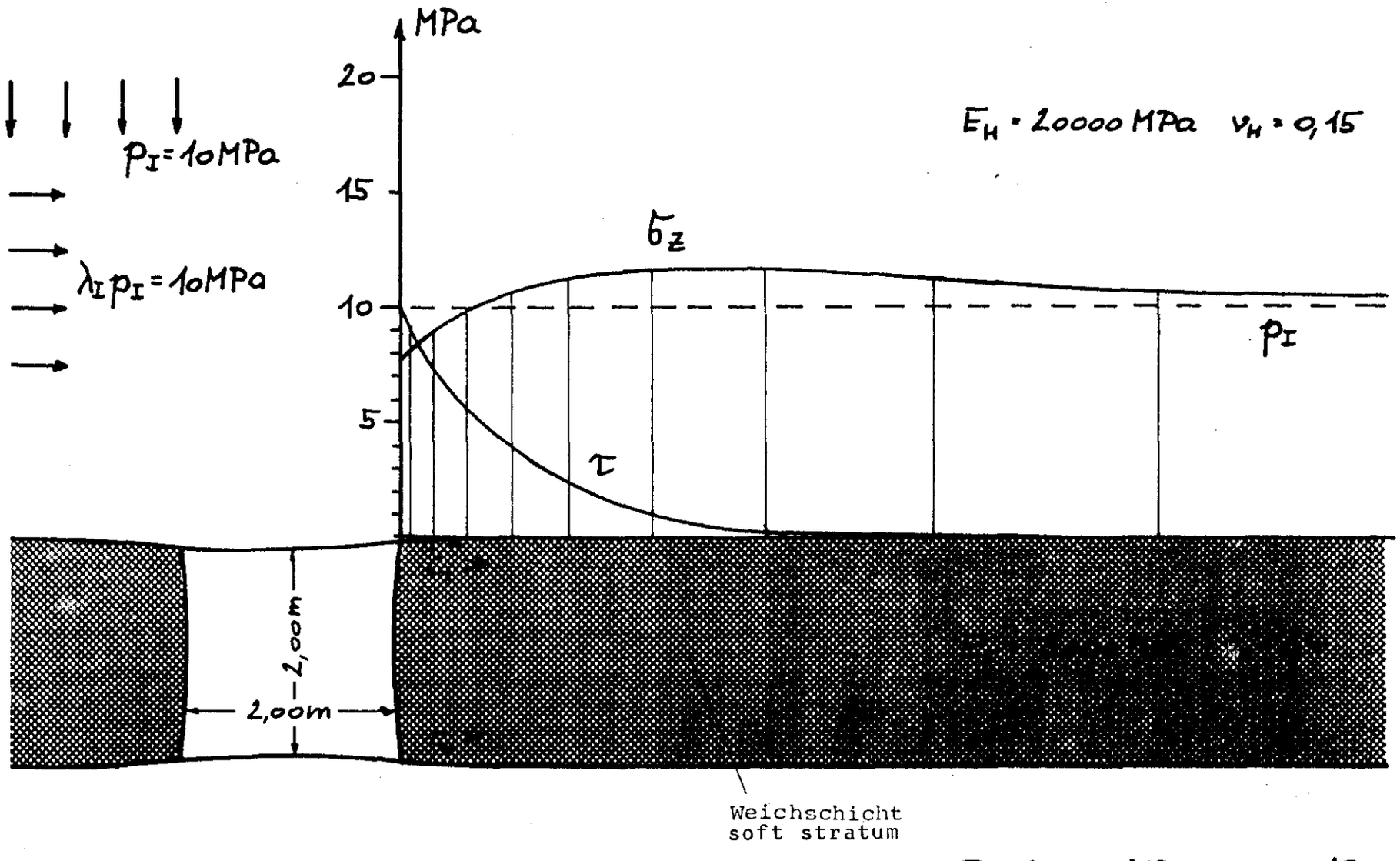
MPa
20
15
10
5
$p_I = 10 MPa$
$\lambda_I p_I = 10 MPa$
σ_z
p_I
τ
2,00m
2,00m
$E_H = 20000 MPa$ $\nu_H = 0,15$
Weichschicht
soft stratum
$E_L = 20000 MPa$ $\nu_L = 0,15$

Abb. 1o

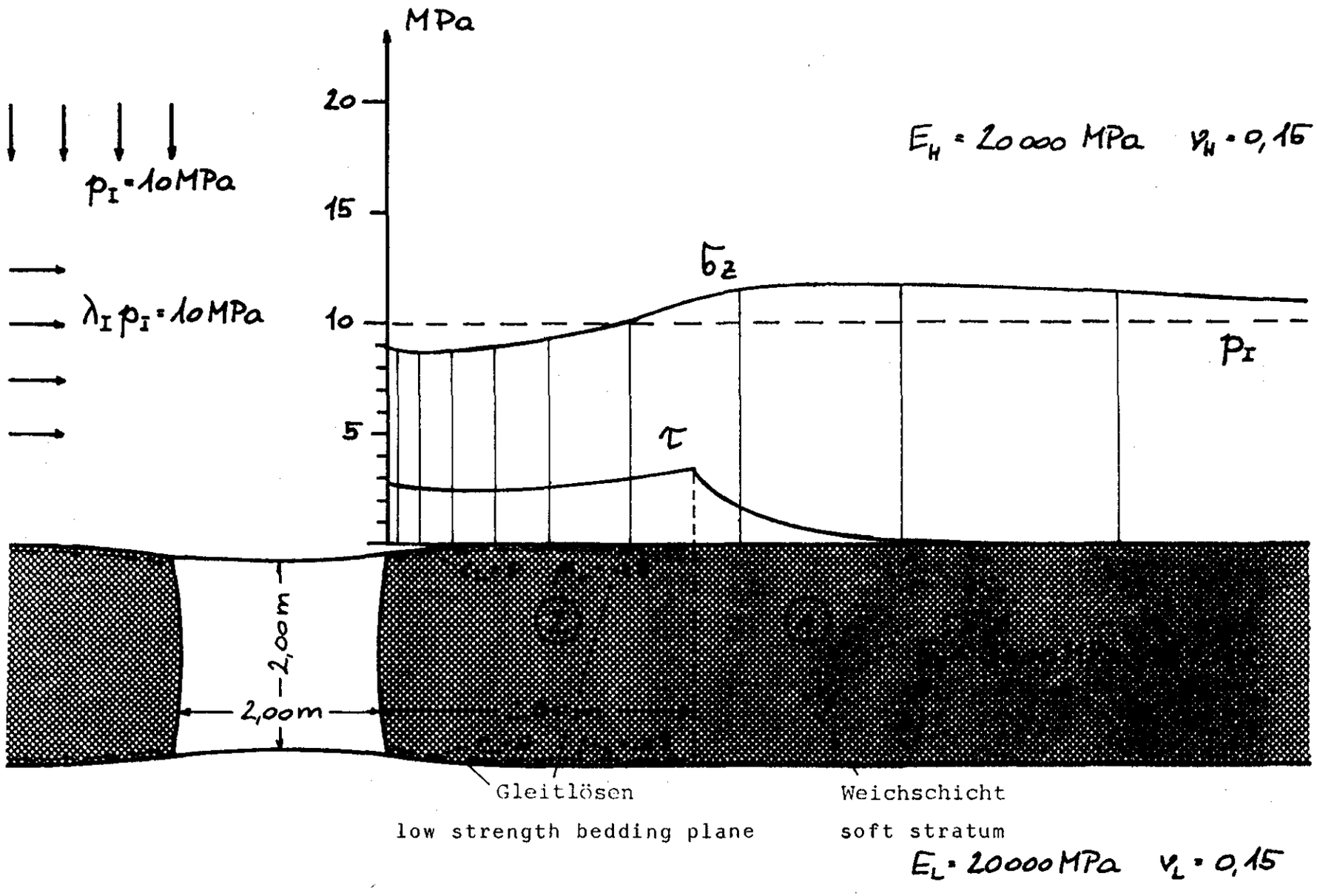
MPa
20
15
10
5
p_I = 10 MPa
$\lambda_I p_I$ = 10 MPa
σ_z
p_I
τ
2,00 m
2,00 m
E_H = 20 000 MPa ν_H = 0,15
Gleitlösen
low strength bedding plane
Weichschicht
soft stratum
E_L = 20000 MPa ν_L = 0,15

Abb. 11

Abb. 12 Flözstrecke auf Niederberg (BRD)
Flöz Gleitling, Teufe: 3oom

Seam roadway on Niederberg (BRD)
Seam Gleitling, depth 3oo m

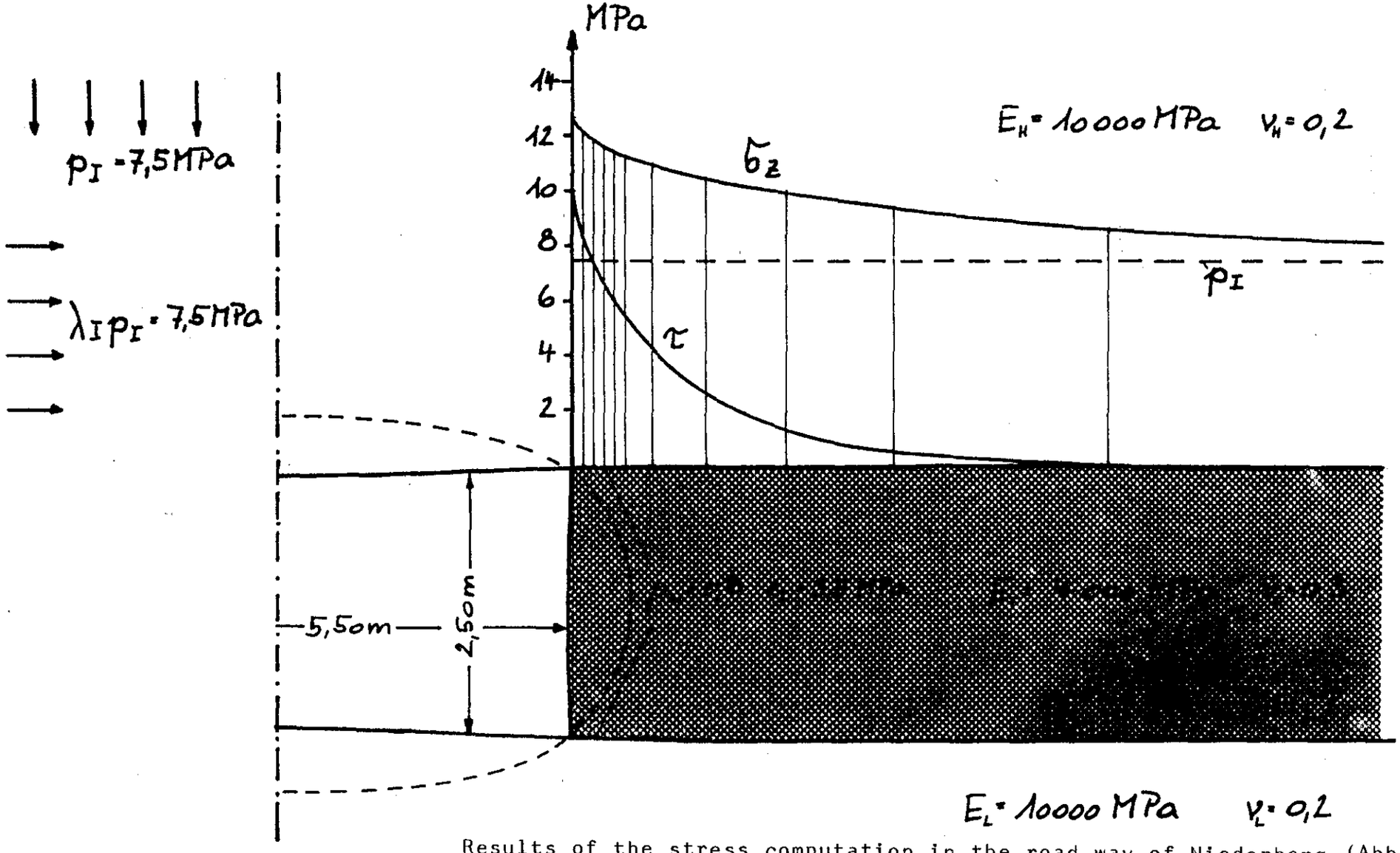

Results of the stress computation in the road way of Niederberg (Abb. 12)

Abb. 13 Ergebnisse der Spannungsberechnung der Flözstrecke auf Niederberg (Abb.12)

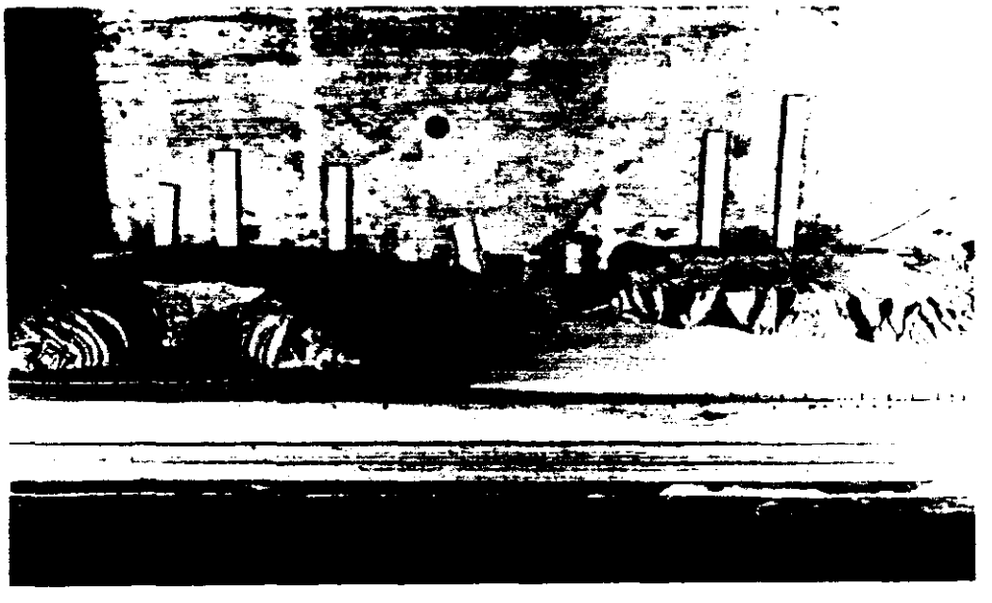

Abb. 14 Modellversuch: Bruchbild zweier Restpfeiler bei unterschiedlicher Reibung zum Begleitgebirge

Model test : failure mechanism of two residual pillars of different friction with the surrounding rock.

ebene Scherflächen bei geringer Reibung

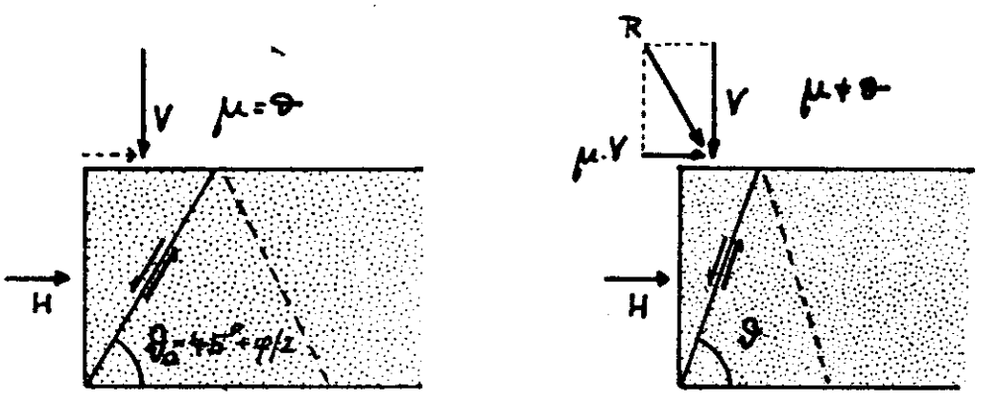

$$\tan\vartheta = \frac{\tan\varphi + \mu + \sqrt{(\tan\varphi + \mu)(\tan\varphi + \cot\varphi)}}{1 - \mu\tan\varphi} \quad (1)$$

φ .... innerer Reibungswinkel
internal angle of friction

$1 - \mu\tan\varphi = 0$ (Nenner Null gesetzt)

denominator = zero

$\mu = \cot\varphi$

$\longrightarrow \mu \geq \cot\varphi \longrightarrow$ keine ebene Scherfläche möglich

no planar shear plane possible

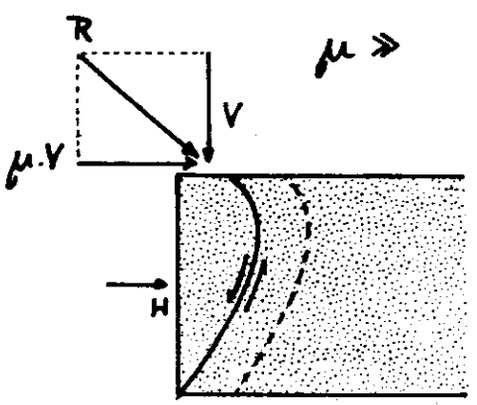

gekrümmte Scherflächen bei großer Reibung zum Begleitgebirge

curved shear planes with great friction to the surrounding rock

Abb. 15 Theoretische Scherflächen bei unterschiedlicher Reibung zum Begleitgebirge

Theoretical shear planes of different friction to the surrounding rock

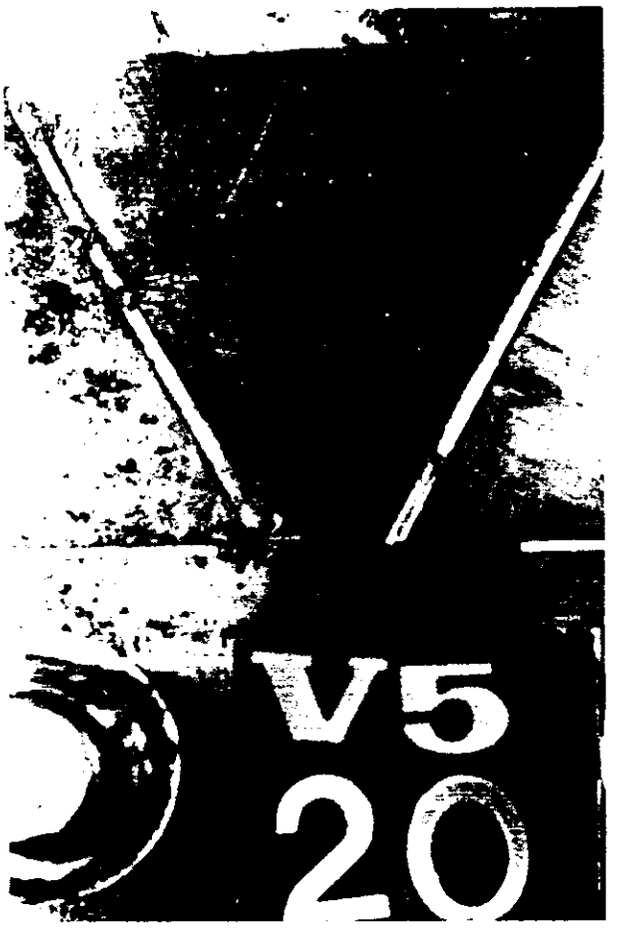

Abb. 17:

Laborversuch: Bruchverhalten der Keilspitze bei aufgezwungener Verformung

Lab. test :

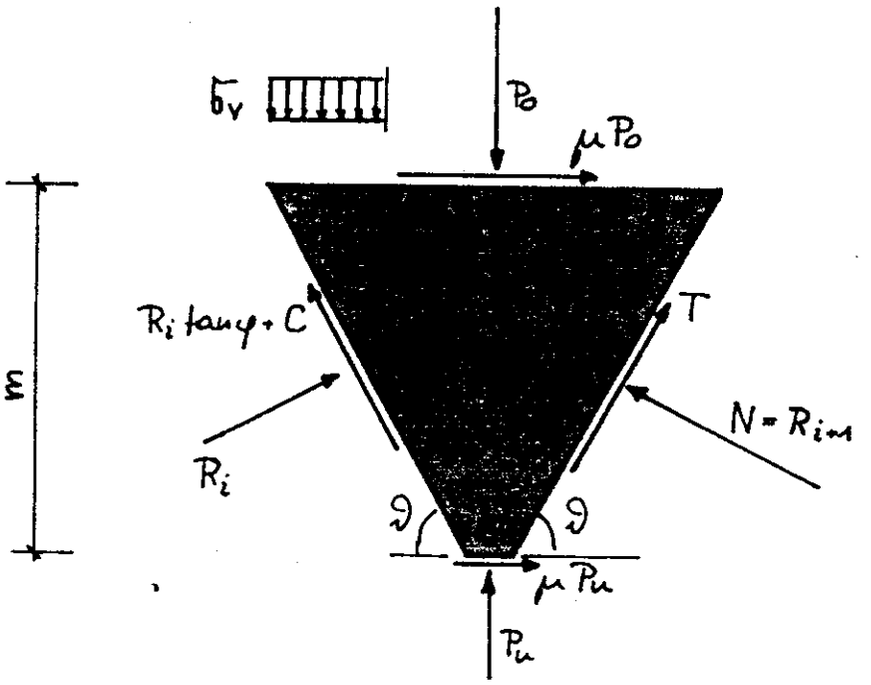

$$N = (P_o - P_u)\cos\vartheta + \mu(P_o + P_u)\sin\vartheta - R_i\cos 2\vartheta - (R_i \tan\varphi + C)\sin 2\vartheta$$

$$T = (P_o - P_u)\sin\vartheta - \mu(P_o + P_u)\cos\vartheta - R_i\sin 2\vartheta + (R_i \tan\varphi + C)\cos 2\vartheta$$

Abb. 16 Gleichgewicht der an einem Bruchkeil angreifenden Kräfte = Rechenansatz für die Keilbruchzone

Equilibrium of forces acting on a failure wedge = computation procedure for the wedge failure zone.

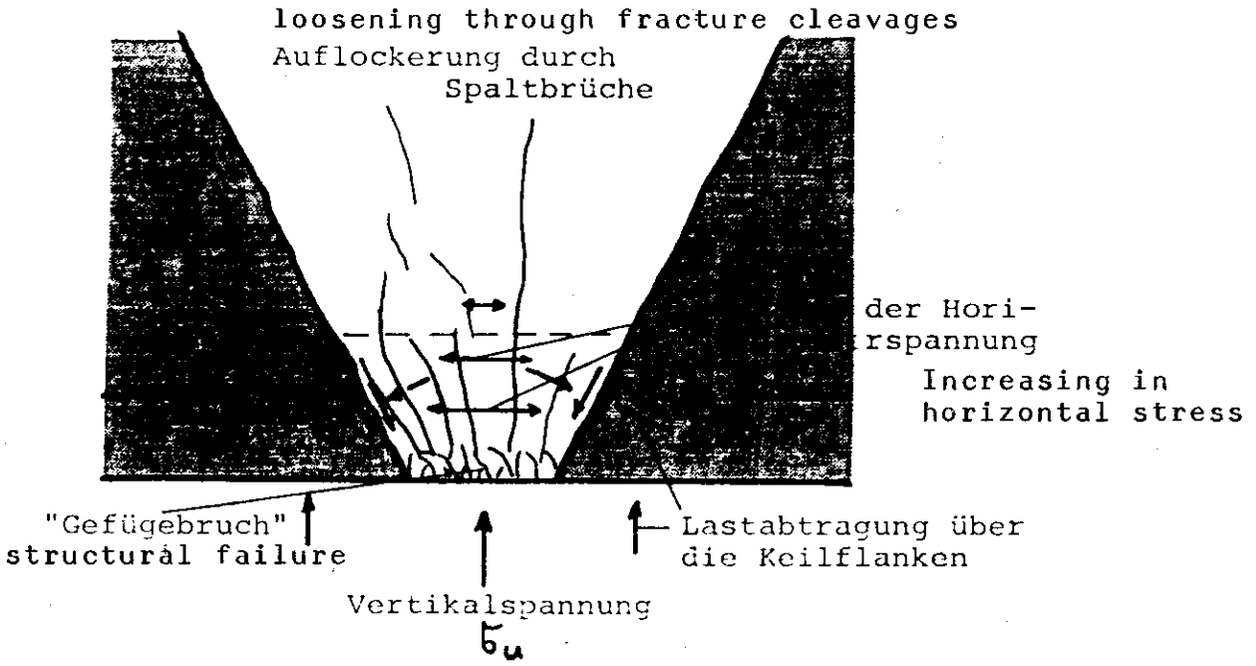

Abb. 18 Bruchmechanismus und Spannungsumlagerungen an der Keilspitze

in the tip of the wedge

Failure mechanism and redistribution of stresses

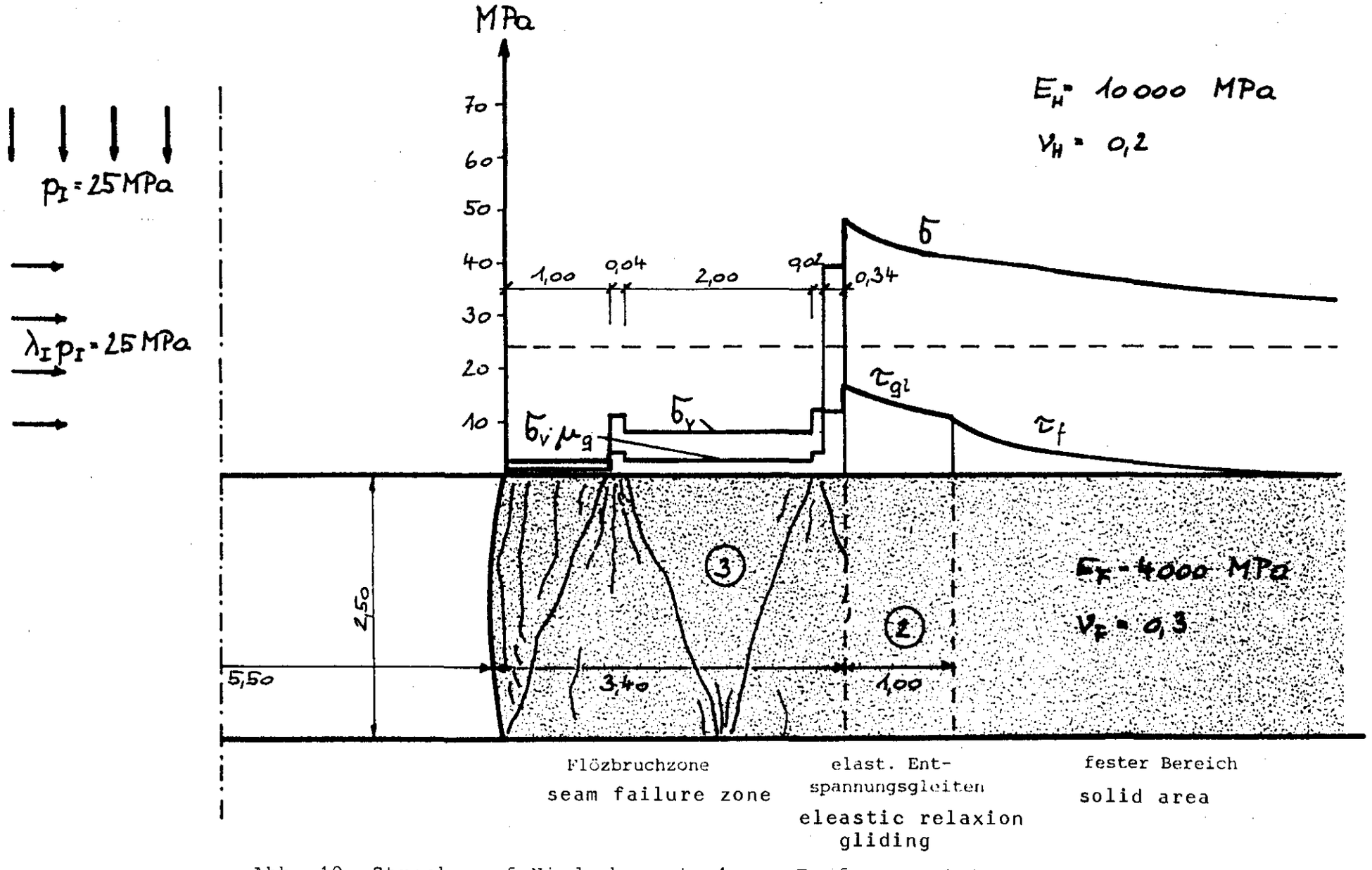

Abb. 19: Strecke auf Niederberg in 1ooom Teufe versetzt: Spannungszustand und Bruchbild im Flöz
Stress state and failure pattern in the seam

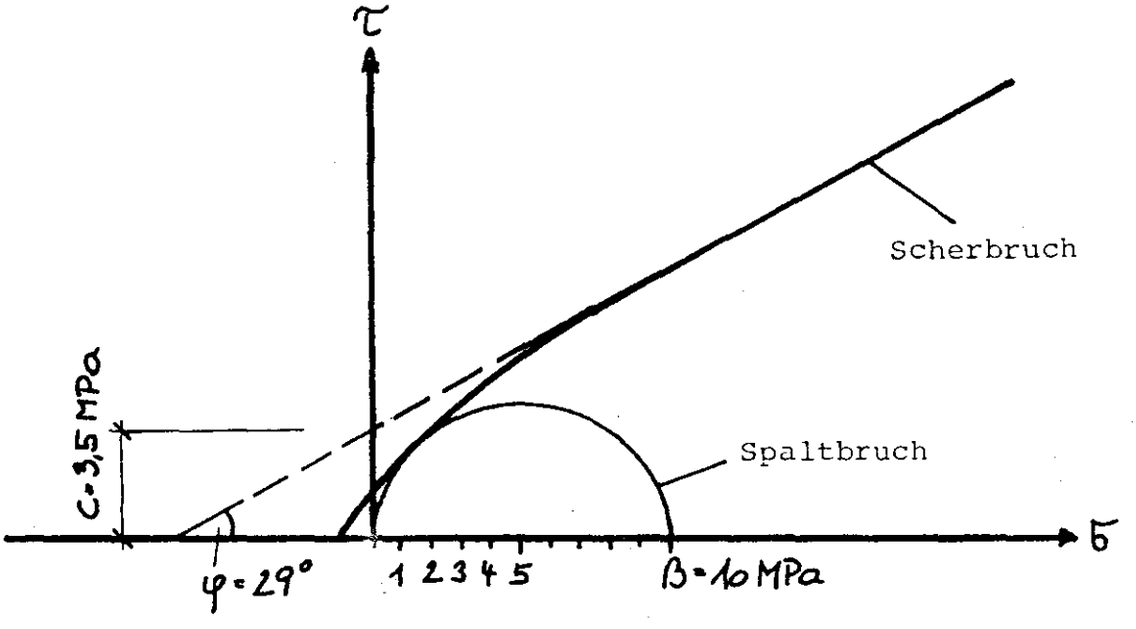

Abb. 2o: Bruchcharakteristik der Kohle (Eingabewerte für die Berechnung der Abb.19)

Failure characteristics of coal (input data for calculation of fig. 19)

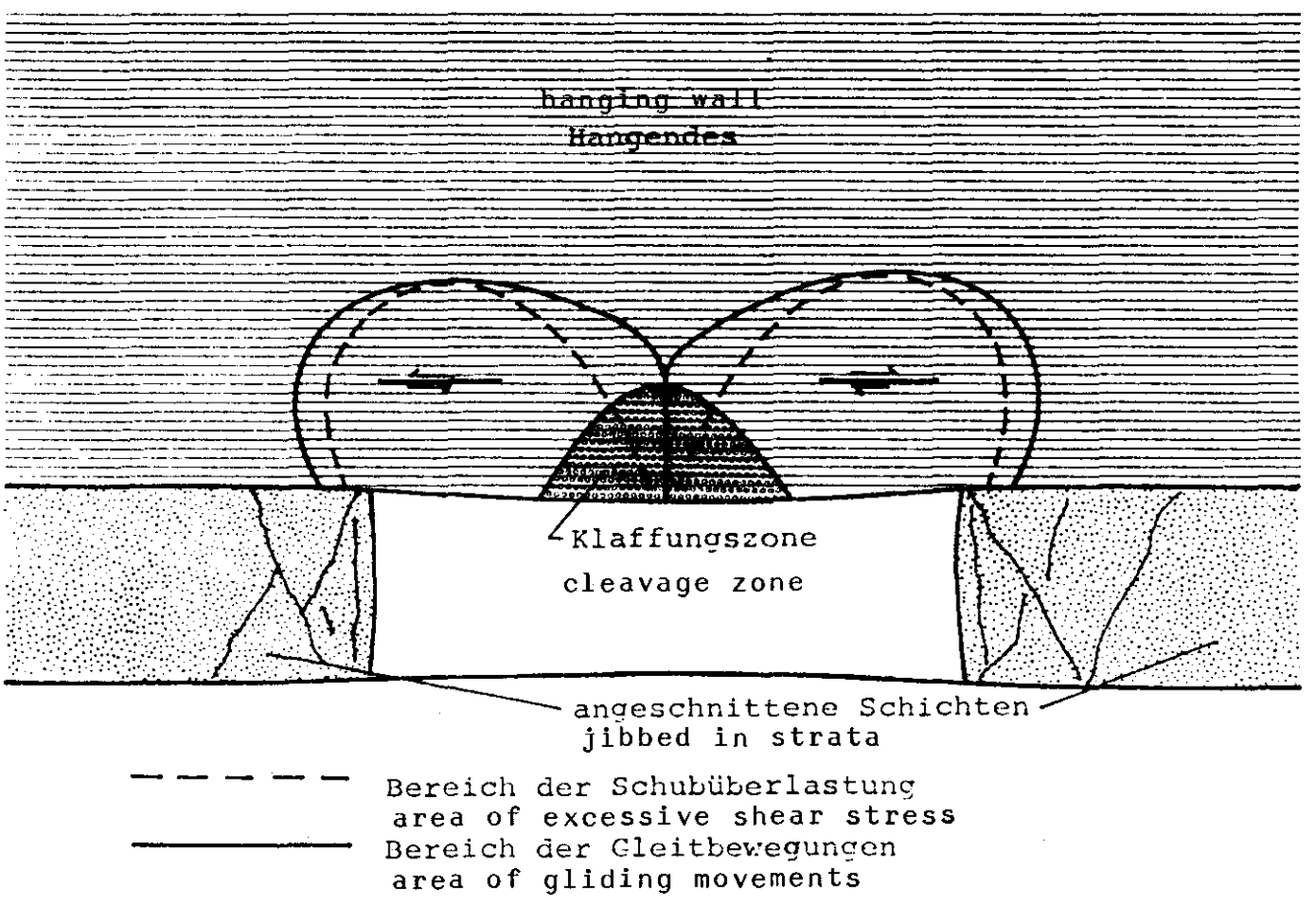

Abb. 21 Firste einer Rechteckstrecke im geschichteten Gebirge: Beeinflussung hohlraumnaher Bereiche durch Gleitlösen (schematisch)

Roof of rectangular roadway in bedding rocks
Influence of low strength bedding planes on areas close to an underground excavation

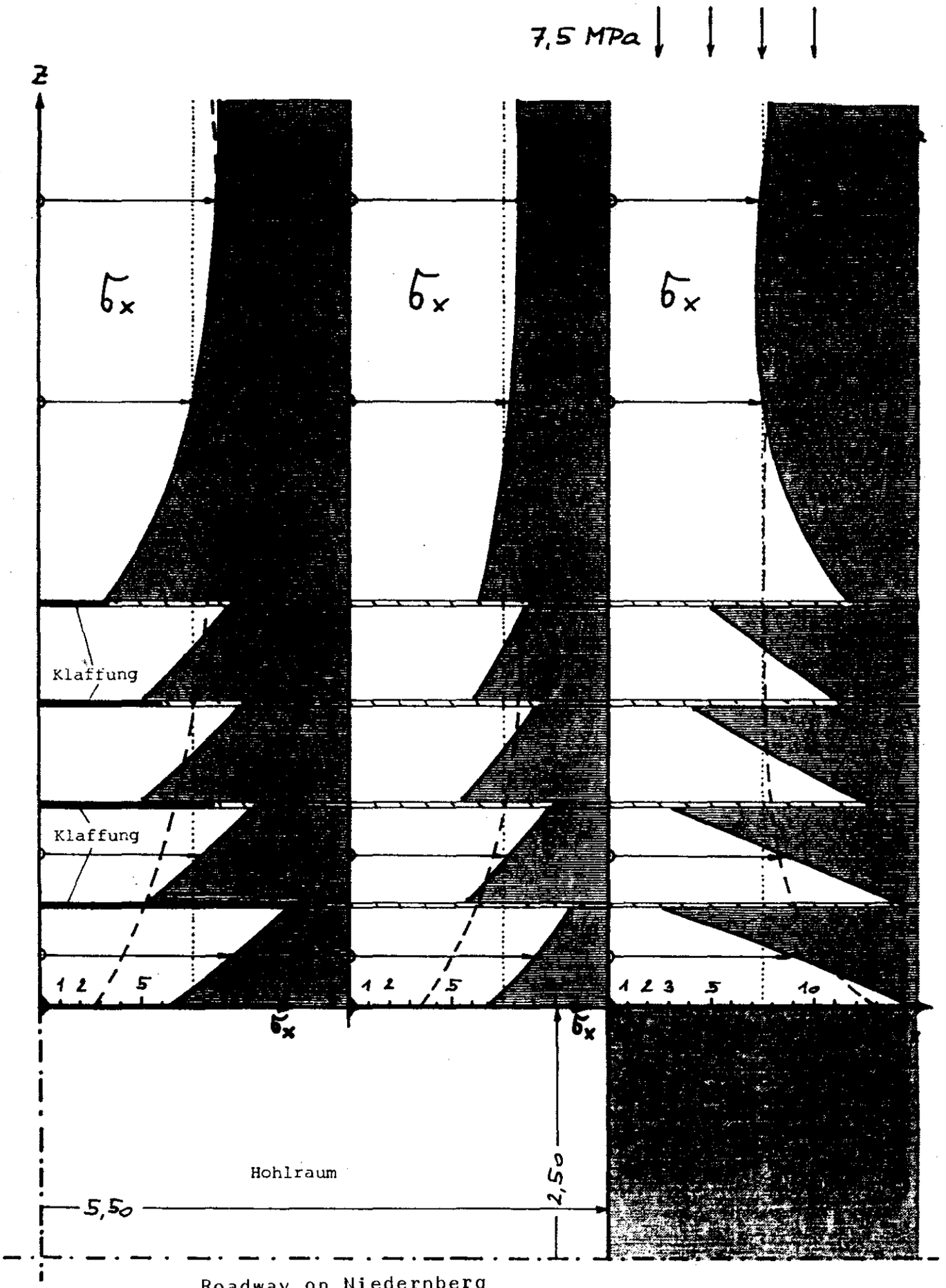

Roadway on Niedernberg

Abb. 22: Strecke auf Niederberg:
Spannungsumlagerungen in der Firste durch 4 Gleitlösen im Abstand von je o,5o m untereinander

Redistribution of stresses in the roof due to 4 low-strength bedding planes (Gleitlösen) o,5o in distance from one another

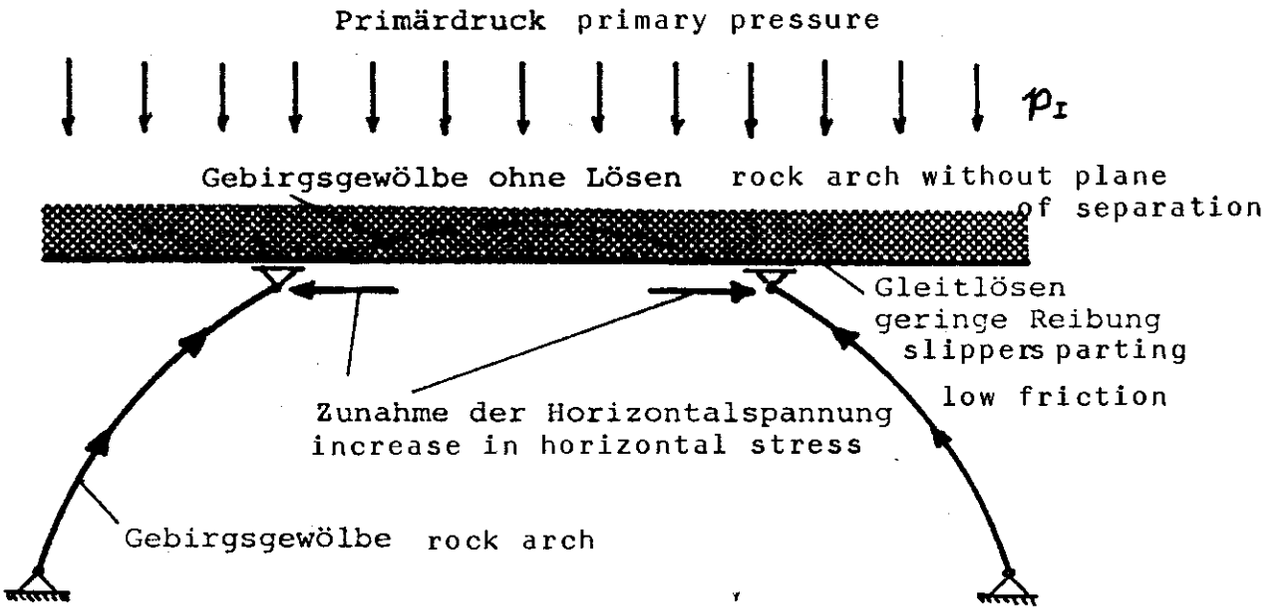

Abb. 23 Störung des natürlichen Gebirgsgswölbes durch ein Gleitlösen und daraus resultierende Spannungsumlagerungen (schematisch)

Disturbance of natural rock arch due to slippers partings and the resulting redistribution of stresses

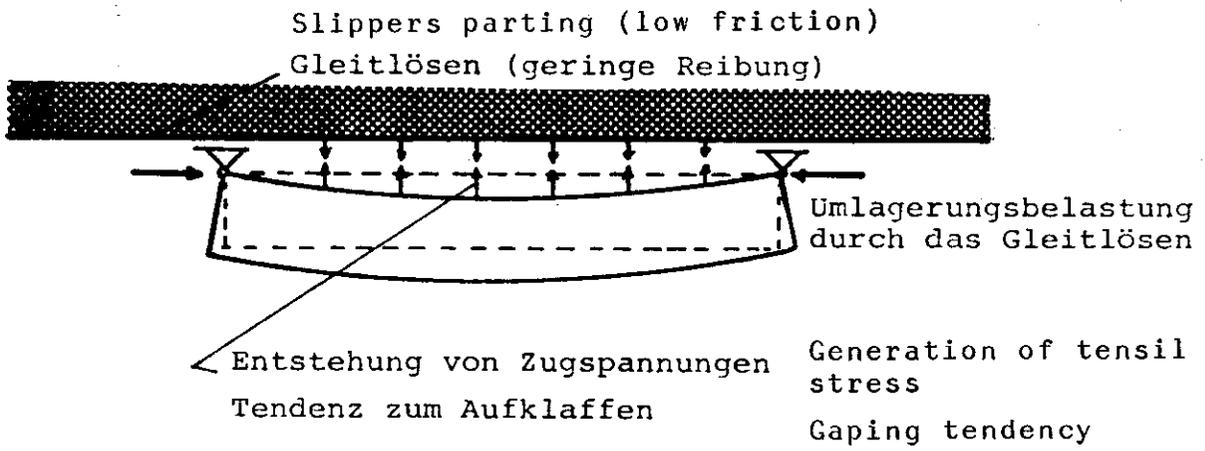

Abb. 24: Entstehung von bankrechten Zugspannungen in hohlraumnahen Schichten infolge der Spannungsumlagerungen durch Schichtgleiten (schematisch)

Generation of tensil stresses normal to the stratification in strata near the excavation due to redsitribution of stresses through gliding.

Abb. 25: Bruchbild einer Strecke mit Hufeisenprofil (Modellversuch des Steinkohlenbergbauvereines Essen (2))

Failure pattern of a roadway with horseshoe profile (model test of the Coal Mining Assoc., Essen (2))

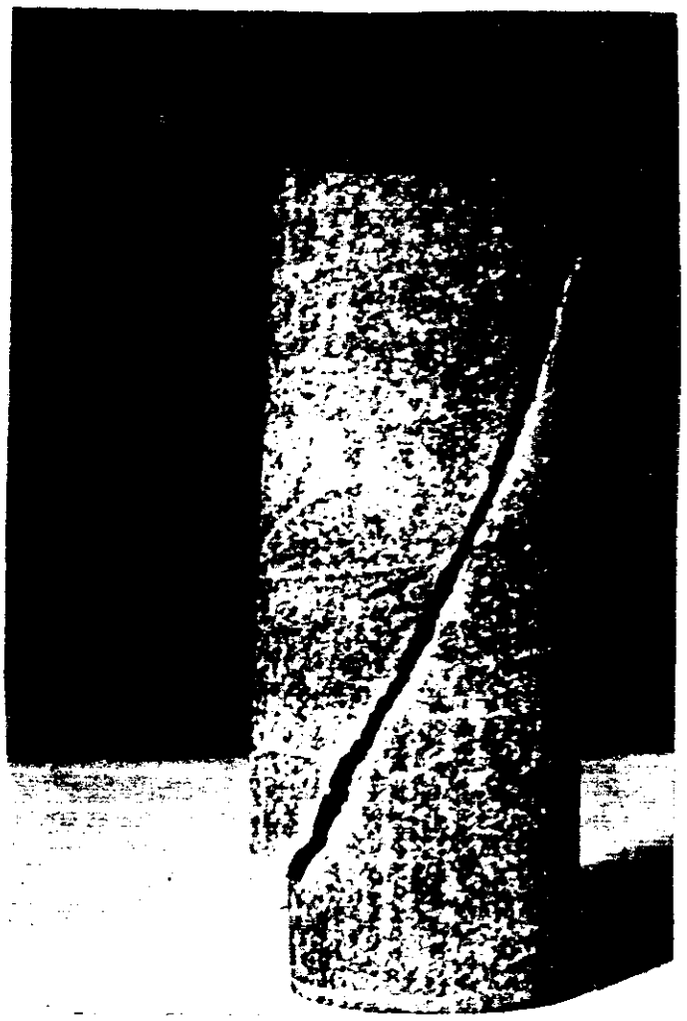

Abb. 26 Bruchbild einer Laborprobe im einachsigen Druckversuch (südafrikanischer Quarzit)

Failure pattern of Lab specimen in uniaxial compressive testing southafrican Quarzite)

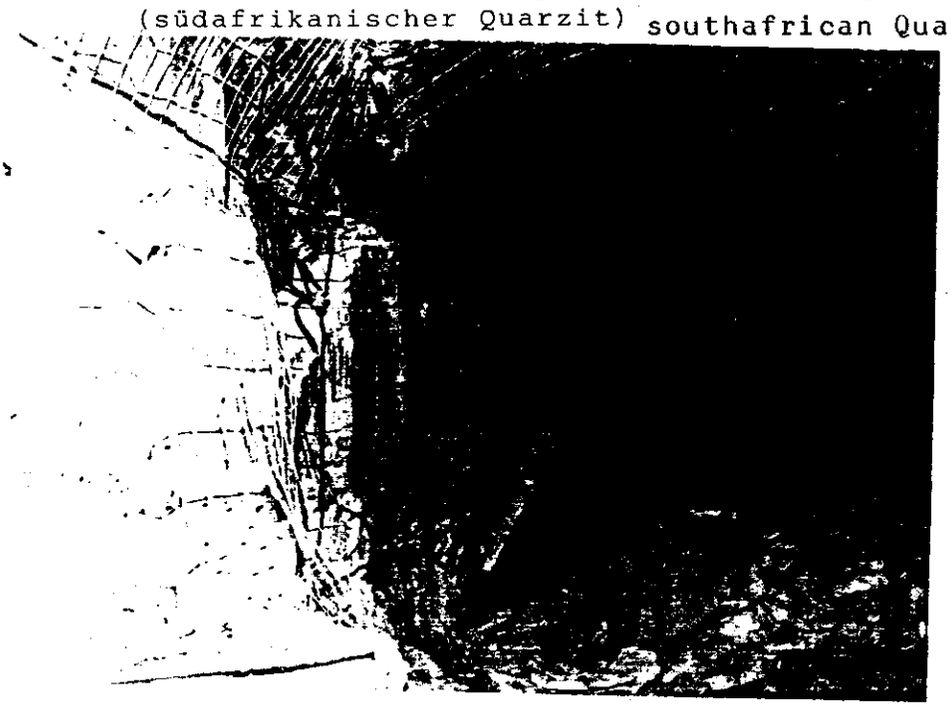

Abb. 27 Bruchbild einer Strecke im südafrikanischen Quarzit: Sprödbruch der Ulmen (slabbing)

Failure pattern of roadway in Southafrican Quarzite : brittle failure (slabbing) of side walls